Technical Report/TR-186-2-98-17 (*14 July 1998*)

New Simple Reflectance Models for Metals and other Specular Materials

László Neumann, Attila Neumann, László Szirmay-Kalos

Department of Control Engineering and Information Technology,
Technical University of Budapest,
Budapest, Műegyetem rkp. 11, H-1111, HUNGARY
Email: szirmay@fsz.bme.hu, neumann@mail.datanet.hu

Abstract

The paper presents new, simple and physically plausible, but not physically based reflectance models for metals and other specular materials. The most important member of this family is the modification of the Phong model, which can eliminate its non-metallic characteristics. The new model gives back the ideal mirror in the limit case, is easier to compute than other known models and is particularly suitable for importance sampling to efficiently generate reflected directions in Monte-Carlo ray-tracing algorithms. Due to its simplicity, the new model can become an integral part of commercial CAD systems to describe the specular part or metallic behavior. The paper also examines the energy balance of the previously known and the newly proposed BRDFs concentrating on the behavior at grazing angles, and comes to the conclusion that the Ward and the Cook-Torrance models cannot guarantee energy balance and thus are not physically plausible. Finally, the generated images demonstrate how the metallic impression can be provided by the new models.

Keywords: Reflectance function, BRDF representation, albedo function, importance sampling

1. Introduction

The most famous BRDF model that can describe specular materials was proposed by Phong [17] and improved by Blinn [3]. This model does not have physical interpretation but is only a mathematical construction. Since the original form violates physics, its corrected version [9][14] is preferred in global illumination algorithms.

The first model that has physical base was proposed by Torrance and Sparrow [20], which was applied in rendering algorithms in [4]. Later, He, Torrance et. al. [7] introduced another model that even more accurately represented the underlying physical phenomena [2]. These models are not suitable for *importance sampling* since it would require the integration and inversion of the probability density functions that are expected to be proportional to the BRDF. Not only is it impossible to compute the required integral and inversion analytically, but even the calculation of BRDF values requires significant computational effort for these physically based models.

In their recent paper Lafortune et. al. approximated a non-linear, metallic BRDF by the combination of modified Phong models [12]. The resulting BRDF is simple, but this approach requires a great number of elementary terms to sufficiently represent highly specular materials. Another drawback of this method is that the BRDF is always bounded for grazing angles.

Radiosity and Monte-Carlo ray-tracing rendering algorithms usually assume that the BRDFs do not violate physics. Such shading models must satisfy both reciprocity and energy balance, and are called *physically plausible* [14].

Reciprocity that was recognized by Helmholtz is the symmetry property of the BRDF (f_r, $[\mathrm{sr}^{-1}]$), which is defined by the following equation [15]:

$$f_r(\mathbf{L}, \mathbf{V}) = f_r(\mathbf{V}, \mathbf{L}), \tag{1}$$

where $\mathbf{L}$ is the unit vector pointing towards the incoming light and unit vector $\mathbf{V}$ defines the viewing direction. Reci-

procity is important because it allows for the backward tracing of the light as happens in ray-tracing algorithms.

Suppose that the surface is illuminated by a beam from direction $\mathbf{L}$. *Energy balance* means that the *albedo*, that is the fraction of the total reflected power cannot be greater than 1:

$$a(\mathbf{L}) = \int_{\Omega} f_r(\mathbf{L}, \mathbf{V}) \cdot \cos\Theta_{\mathbf{V}} \, d\omega_{\mathbf{V}} \leq 1. \qquad (2)$$

Energy balance makes the linear operator of the rendering equation a contraction, which is usually required by iterative and random walk methods to converge to the solution.

For the representation of metals, there has been no simple, physically plausible model so far that is also good for highly specular materials and can give back the mirror as the limit case. This paper intends to fill this gap.

2. Metals and Phong-type models

2.1. Properties of metals and mirrors

Metals have several important properties:

- Their diffuse reflectance is usually negligible.
- The color reflected off the metals is determined by the Fresnel function. Due to the angle dependence of the Fresnel function, this color fades at grazing angles.
- If the surface roughness goes to zero, metals become shinier and converge to the *ideal mirror*. The reflectance function of the ideal mirror is $\delta \cdot F(\Theta)/\cos\Theta_{\mathbf{L}}$, where δ is the Dirac-delta, F is the Fresnel function and $\Theta_{\mathbf{L}}$ is the incident angle. If the Fresnel term of the material is 1, then an ideal mirror would reflect all energy independently of the illumination, that is the albedo is 1 and the reflected radiance is equal to the corresponding input radiance. At directions other than the reflection direction, the radiance is zero. As the material properties converge to that of the ideal mirror, both the *energy reflectivity* (albedo) and the *radiance reflectivity* (BRDF) are expected to converge to the corresponding functions of the ideal mirror.
- The BRDF function of metals has $1/\cos\Theta_{\mathbf{L}}$ characteristics that can compensate for the $\cos\Theta_{\mathbf{L}}$ factor of the irradiance.
- For great incident angles, the peak of the reflection lobe (so called off-specular peak) occurs at an angle greater than the angle of incidence.

When the new models are compared to the different versions of the Phong model, these properties are examined. We shall conclude that the new models meet all but the last requirements.

Let us consider the specular part of the physically plausible versions of the Phong and the Blinn models [14]. Using the widely accepted notations where $\mathbf{R}$ is the mirror direction of $\mathbf{L}$, $\mathbf{N}$ is the unit normal vector, and $\mathbf{H}$ is the halfway unit vector between $\mathbf{L}$ and the view vector $\mathbf{V}$, the Phong and Blinn models are defined as the nth power of the dot products $(\mathbf{R}\cdot\mathbf{V})$ and $(\mathbf{N}\cdot\mathbf{H})$, respectively. For large n values the BRDF gets highly specular. However, these models cannot provide metallic or mirror looking since as the incident angle grows towards the grazing angle, the ratio of the reflected power as well as the output radiance decrease. If n goes to infinity, then the reflected radiance and the albedo converges to zero for 90 degree incident angle since in this limit case the albedo follows the cosine function. Intuitively, the decrease of the radiance means that if we look at a Phong-mirror, then the image reflected in the mirror gets darker for greater reflection angles.

2.2. The new model for metals

This section discusses a construction method which preserves the reciprocity and the energy balance of the BRDF, but solves the mentioned problems of Phong-type models.

Considering the limit case, we should realize that in order to eliminate the undesired behavior of the Phong model, its cosine term must be compensated by an $1/\cos\Theta_{\mathbf{L}}$ factor. However, if we multiplied the specular part of the reciprocal Phong model [13] by $1/\cos\Theta_{\mathbf{L}}$, then we would get back the original, non-reciprocal Phong [17] expression. On the other hand, if we multiplied it with $1/(\cos\Theta_{\mathbf{L}} \cdot \cos\Theta_{\mathbf{V}})$, then the radiance would be unacceptably high around the reflection direction at grazing angles and the energy balance could not be preserved. We can come to the same conclusion with $1/\sqrt{(\cos\Theta_{\mathbf{L}} \cdot \cos\Theta_{\mathbf{V}})}$ [21] correction factor as well.

However, the $1/\max(\cos\Theta_{\mathbf{L}}, \cos\Theta_{\mathbf{V}})$ function have been found appropriate. Let the minimum of the incident and the viewing angles be $\Theta_{\min}$:

$$\Theta_{\min} = \min(\Theta_{\mathbf{L}}, \Theta_{\mathbf{V}}). \qquad (3)$$

The proposed correction term is

$$\frac{1}{\cos\Theta_{\min}} = \frac{1}{\max(\cos\Theta_{\mathbf{L}}, \cos\Theta_{\mathbf{V}})}. \qquad (4)$$

Let $\cos\alpha = (\mathbf{R}\cdot\mathbf{V})^+$ where $(\mathbf{R}\cdot\mathbf{V})^+ = (\mathbf{R}\cdot\mathbf{V})$ if $(\mathbf{R}\cdot\mathbf{V}) \geq 0$ and 0 otherwise. The BRDF of the reciprocal Phong model is

$$f_{r,\mathrm{Phong}}(\mathbf{L}, \mathbf{V}) = c_n \cdot \cos^n \alpha \qquad (5)$$

where c_n is a scalar parameter. Lafortune [13] has shown that

$$c_n \leq \frac{n+2}{2\pi} \qquad (6)$$

must hold in order for the model to preserve energy balance.

The new, corrected, reciprocal BRDF, which is the main result of this paper, is

$$\boxed{f_r(\mathbf{L}, \mathbf{V}) = c_n \cdot \frac{\cos^n \alpha}{\cos\Theta_{\min}}.} \qquad (7)$$

This model meets the mentioned requirements and really provides metallic impression as we demonstrate it later.

Since the reflection vector $\mathbf{R}$ is

$$\mathbf{R} = 2(\mathbf{N} \cdot \mathbf{L})\mathbf{N} - \mathbf{L}, \tag{8}$$

the formula to compute $(\mathbf{R} \cdot \mathbf{V})$ can be expressed as

$$(\mathbf{R}\cdot\mathbf{V}) = (2(\mathbf{N}\cdot\mathbf{L})\mathbf{N} - \mathbf{L})\cdot\mathbf{V} = 2(\mathbf{N}\cdot\mathbf{L})(\mathbf{N}\cdot\mathbf{V}) - (\mathbf{L}\cdot\mathbf{V}). \tag{9}$$

Substituting this into equation 7, we can obtain the following formula for the new BRDF:

$$f_r(\mathbf{L},\mathbf{V}) = c_n \cdot \frac{[(2(\mathbf{N}\cdot\mathbf{L})(\mathbf{N}\cdot\mathbf{V}) - (\mathbf{L}\cdot\mathbf{V}))^+]^n}{\max((\mathbf{N}\cdot\mathbf{L}),(\mathbf{N}\cdot\mathbf{V}))}. \tag{10}$$

The albedo function of the new model can be computed from the Phong BRDF as the sum of the following two integrals:

$$a(\mathbf{L}) = \int\limits_{\Omega((\mathbf{N}\cdot\mathbf{L}))<(\mathbf{N}\cdot\mathbf{V}))} f_{r,\mathrm{Phong}}(\mathbf{L},\mathbf{V})\, d\omega_{\mathbf{V}} + \int\limits_{\Omega((\mathbf{N}\cdot\mathbf{L})\geq(\mathbf{N}\cdot\mathbf{V}))} f_{r,\mathrm{Phong}}(\mathbf{L},\mathbf{V}) \cdot \frac{(\mathbf{N}\cdot\mathbf{V})}{(\mathbf{N}\cdot\mathbf{L})}\, d\omega_{\mathbf{V}}. \tag{11}$$

Analyzing the albedo functions we can come to the conclusion that the c_n constant of inequality 6 is also good for the new model. More precisely, the albedo of the BRDF of equation 7 has only a negligible overshooting where it exceeds value 1 if $n \geq 1$. The overshooting occurs at small incident angles where $\mathbf{L}$ is close to $\mathbf{N}$.

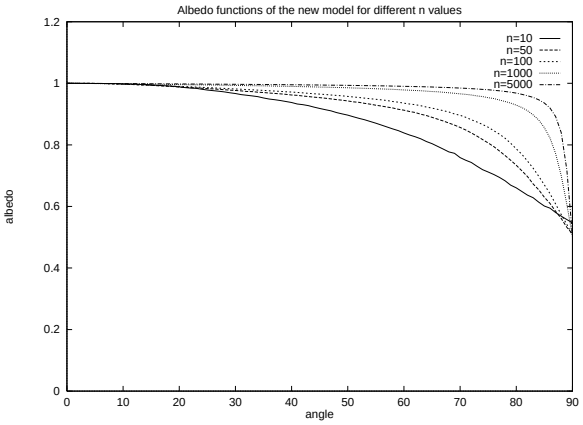

Figure 1: *Albedo functions of the new model for different n values*

Below the arbitrarily selected $n = 1$ minimum, the c_n value should be decreased in order to preserve energy balance, which would shift the maximum of the albedo function and the BRDF from the perpendicular incident direction. For example, if $n = 1$ or 0.5, then the maximum c_n constant would result in 0.0003, and 0.01 maximum overshooting at 13 and 30 degrees, respectively.

Figure 1 shows the albedo functions for different n values. We can see that in the limit case the albedo converges to constant 1, which is the albedo of the ideal mirror.

2.3. Transition from the Phong model to the new model: p-model

Using a $p \in [0,1]$ parameter, a continuous transition can be developed between the reciprocal Phong model defined by equation 5 and the new metal model, as follows:

$$f_r(\mathbf{L},\mathbf{V}) = c_n \cdot \frac{\cos^n \alpha}{\cos^p \Theta_{\min}}, \qquad 0 \leq p \leq 1. \tag{12}$$

Let us call this formula the p-model. If $n \geq 1$, then the maximum of the multiplicative factor c_n is as shown in equation 6 for any $p \in [0,1]$.

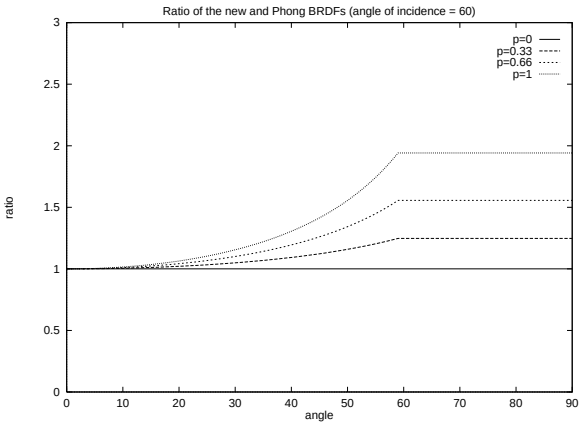

Figure 2: *Ratio of the p-model and the Phong BRDFs for different viewing angles*

Figure 2 shows the ratio of the BRDFs of the p-model and the Phong model for different viewing angles $\Theta_{\mathbf{V}}$ and for different transition parameters p. The case of $p = 0$ represents the reciprocal Phong model, while the case of $p = 1$ means the new metal model.

2.4. The properties of the new metal model

This section examines the properties of the new model. Figure 3 compares the specular lobes of the Phong, new, Cook-Torrance and He-Torrance models at 42° incident angle. The models have been calibrated to provide similar response for perpendicular illumination.

Supposing that the Fresnel term is 1 (for silver this is practically true), the albedos of the Phong, He-Torrance, Cook-Torrance, Ward and the new models are shown in figure 4. Note that the Cook-Torrance and the Ward models diverge at grazing angles, while the Phong, He-Torrance and Ward BRDFs badly decrease for greater incident angles. The new model converges to a value that is not lower than 0.5 for grazing angles.

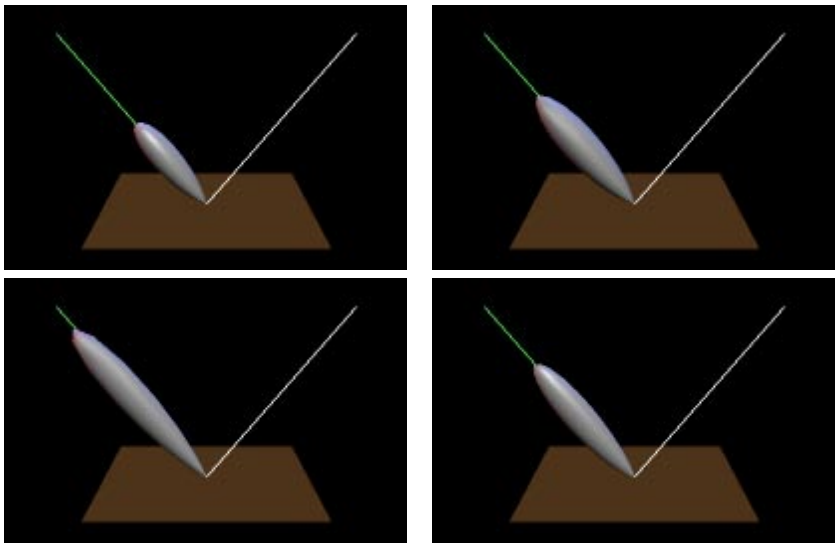

Figure 3: *Specular lobes of the Phong ($n = 20$), new ($n = 20$), Cook-Torrance ($m = 0.1,\ n = 5$) and He-Torrance ($\sigma_0 = 0.1,\ \tau = 1.4,\ n_i = 6,\ n_r = 0.8$) models*

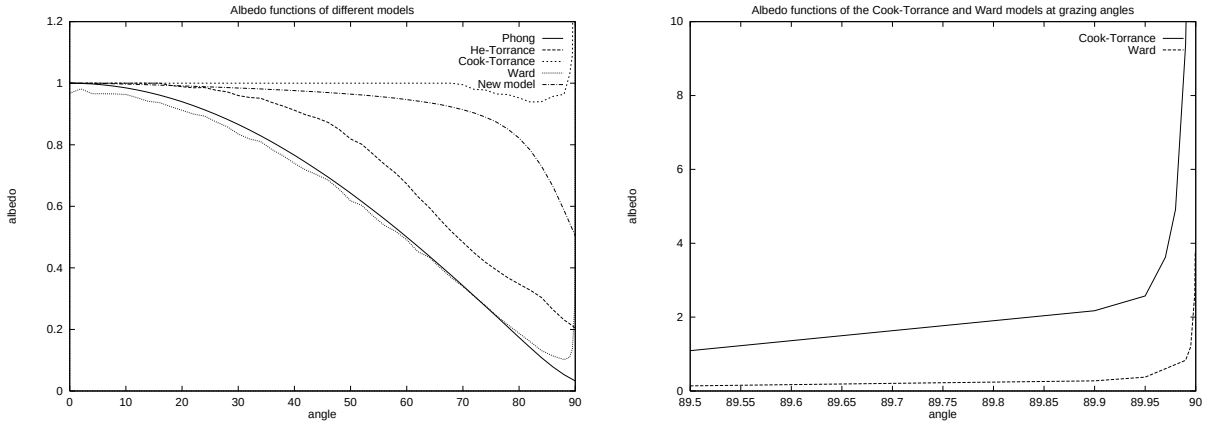

Figure 4: *Albedo functions of the Phong ($n = 150$), new ($n = 150$), Cook-Torrance ($m = 0.1$), Ward ($m = 0.1$) and He-Torrance ($\sigma_0 = 0.1,\ \tau = 1.7$) models*

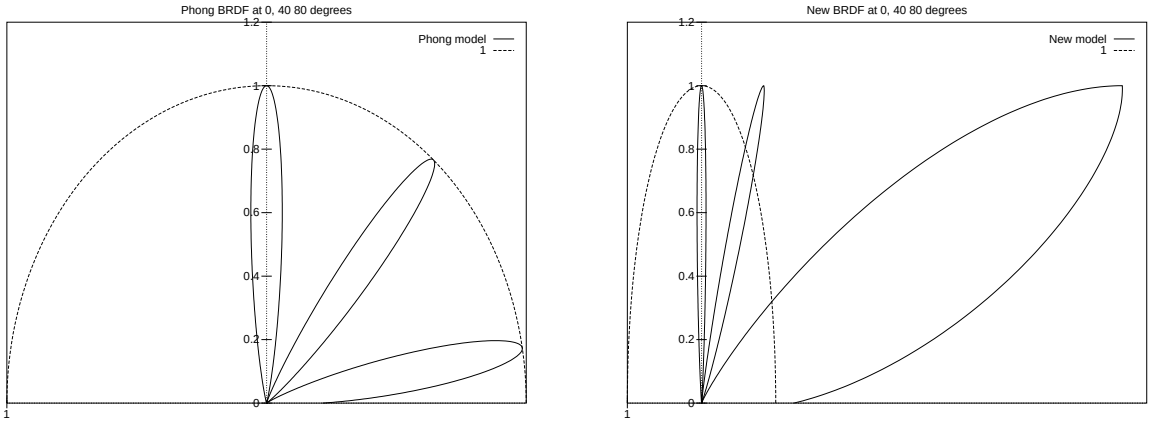

Figure 5: *Comparison of the BRDFs of the Phong and the new models ($n = 100$)*

The maximum of the new BRDF is always at the mirror direction $\mathbf{R}$ and its value is $c_n / \cos\Theta_{\mathbf{L}}$ for any n, while the maximum of the Phong model is always c_n.

Figure 5 compares the normalized BRDF functions of the Phong and the new models for 0, 40 and 80 degree incident angles (normalization scales the BRDF to be 1 at 0 incident angle).

It is also worth examining the output radiance assuming a single point-like lightsource of intensity 4π at distance 1 in direction $\mathbf{L}$. In this case the irradiance is $\cos\Theta_{\mathbf{L}}$. The output radiances of the Phong and the new models at different incident directions are shown in figure 6. This figure demonstrates the earlier statement that the "Phong-mirror" gets darker for greater incident angles, but the new model eliminates this artifact.

2.4.1. Behavior at grazing angles

The new model slightly differs from real metals at grazing angles. Unfortunately no reliable data are available about the reflection of metals around 90 degree incident angle. However, when the He-Torrance model was fitted, the following observation was made [11]: The normalized BRDF has about 1 value at the mirror direction while the maximum which is of order $1/\cos\Theta_{\mathbf{L}}$ is significantly below the mirror direction (off-specular peak). Although this feature is not included in the new model, according to our experience this error is not visually observable.

2.4.2. Ideal mirror

The new model gives back the normalized BRDF of the ideal mirror for $n \to \infty$, which is $1/\cos\Theta_{\mathbf{L}}$. The output radiance is $L^{\text{out}}(\mathbf{V}) = L^{\text{in}}(\mathbf{L})$ if $\mathbf{V} = \mathbf{L}$ and 0 otherwise.

Note that the new model can arbitrarily approximate the ideal mirror. Selecting n in an appropriate way (e.g. $n = 10^4 \ldots 10^8$), realistic, glossy mirrors can easily be generated. Using, for example, distributed ray-tracing, the mirrors do not require a special case.

3. Generalizations of the new model

3.1. Retro-reflective materials

The proposed model can easily be generalized to provide a *retro-reflective* BRDF which has the maximum at the direction of the incident illumination. Practical examples of retro-reflective objects are a projection screen, a traffic sign, etc. For retro-reflective materials, mirror direction vector $\mathbf{R}$ should be replaced by the illumination direction $\mathbf{L}$. The BRDF formula can be simplified to the following form:

$$f_r(\mathbf{L},\mathbf{V}) = c_n \cdot \frac{[(\mathbf{L}\cdot\mathbf{V})^+]^n}{\max((\mathbf{N}\cdot\mathbf{L}),(\mathbf{N}\cdot\mathbf{V}))}. \qquad (13)$$

The maximum value of c_n is as defined in equation 6.

3.2. Anisotropic materials

Lafortune et. al. [12] introduced the anisotropic generalization of the Phong model as:

$$f_r(\mathbf{L},\mathbf{V}) = C_{\max}\cdot(C_x(R_xV_x)+C_y(R_yV_y)+C_z(R_zV_z))^n = C_{\max}\cdot[(\mathbf{R}\cdot\mathbf{V})_M]^n, \qquad (14)$$

where $(\mathbf{R}\cdot\mathbf{V})_M = \mathbf{R}^{\mathrm{T}} M \mathbf{V}$ is a special dot product containing also a multiplication with diagonal matrix M. The values at the diagonal of M are C_x, C_y and C_z, respectively.

As for the original Phong model, the anisotropic generalization can also be normalized with p-th power of the maximum of the dot products $(\mathbf{N}\cdot\mathbf{L})$, $(\mathbf{N}\cdot\mathbf{V})$, thus we can obtain:

$$f_r(\mathbf{L},\mathbf{V}) = C_{\max}\cdot\frac{[(\mathbf{R}\cdot\mathbf{V})_M]^n}{\max((\mathbf{N}\cdot\mathbf{L}),(\mathbf{N}\cdot\mathbf{V}))^p}. \qquad (15)$$

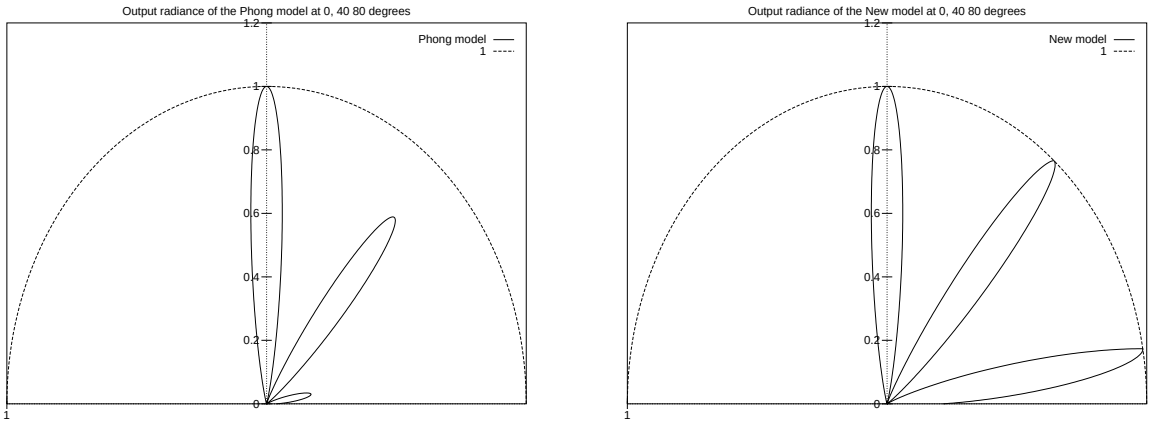

Figure 6: *Comparison of the output radiances of the Phong and the new models ($n = 100$)*

This model is able to approximate metals even with a single term, but several terms can also be combined together. The resulting approximation is better than Lafortune's scheme since letting $p = 0$ this formula gives back his original expression as a special case. The general formula containing a combination of several terms is:

$$f_r(\mathbf{L}, \mathbf{V}) = \sum_i C_i \cdot \frac{[(\mathbf{R} \cdot \mathbf{V})_{M_i}]^{n_i}}{\max((\mathbf{N} \cdot \mathbf{L}), (\mathbf{N} \cdot \mathbf{V}))^{p_i}}. \quad (16)$$

4. Importance sampling

Importance sampling is an effective technique to reduce the variance of Monte-Carlo algorithms. It requires the generation of random samples according to a probability density which is proportional, or at least approximately proportional to the integrand.

In order to generate the output radiance $L^{\text{out}}(\mathbf{V})$ from the incident illumination $L^{\text{in}}(\mathbf{L})$ ($\mathbf{L} \in \Omega$) in Monte-Carlo ray-tracing, the following integral should be evaluated:

$$L^{\text{out}}(\mathbf{V}) = \int_\Omega L^{\text{in}}(\mathbf{L}) \cdot f_r(\mathbf{L}, \mathbf{V}) \cdot \cos\Theta_{\mathbf{L}} \, d\omega_{\mathbf{L}}. \quad (17)$$

If $p(\mathbf{L})$ is a probability density and directions $\mathbf{L}_1, \mathbf{L}_2, \ldots, \mathbf{L}_M$ are sampled following this probability distribution, then the Monte-Carlo estimate of this integral is:

$$L^{\text{out}}(\mathbf{V}) \approx \frac{1}{M} \cdot \sum_{m=1}^{M} L^{\text{in}}(\mathbf{L}_m) \cdot \frac{f_r(\mathbf{L}_m, \mathbf{V}) \cdot \cos\Theta_{\mathbf{L}_m}}{p(\mathbf{L}_m)}. \quad (18)$$

According to the concept of *importance sampling*, $p(\mathbf{L})$ should be approximately proportional to the integrand to minimize the variance of the solution. If no a-priori information is available about L^{in}, then it is assumed to be constant, thus the probability density should be proportional to $f_r(\mathbf{L}, \mathbf{V}) \cdot \cos\Theta_{\mathbf{L}}$.

4.1. Importance sampling for the Phong model

For the Phong model where the integrand is

$$L^{\text{in}}(\mathbf{L}) \cdot c_n \cdot (\mathbf{V} \cdot \mathbf{R})^n \cdot \cos\Theta_{\mathbf{L}} = L^{\text{in}}(\mathbf{L}) \cdot c_n \cdot \cos^n \alpha \cdot \cos\Theta_{\mathbf{L}},$$

Lafortune [13] proposed the following probability density:

$$p(\mathbf{L}) = \frac{n+1}{2\pi} \cdot [(\mathbf{V} \cdot \mathbf{R})^+]^n = \frac{n+1}{2\pi} \cdot \cos^n \alpha. \quad (19)$$

Samples according to this probability density can be generated in the following way. Suppose that we can get (u_m, v_m) samples from a set containing uniformly distributed points in the unit square. Note that this sampling will be used in Monte-Carlo ray-tracing where rays are traced backwards. It means that for a given $\mathbf{V}$ an appropriate $\mathbf{L}$ vector should be found, which consists of two steps. In the first step reflection direction $\mathbf{R}_m$ is found, then $\mathbf{L}_m$ is generated by mirroring.

In order to find a reflection direction $\mathbf{R}_m$, angles α_m and ϕ_m in the lobe around $\mathbf{V}$ is generated:

$$(\alpha_m, \phi_m) = (\arccos u_m^{\frac{1}{n+1}}, 2\pi v_m). \quad (20)$$

Note that using this formula, the probability density of generating a given direction (α, ϕ) is $\frac{(n+1)}{2\pi} \cos^n \alpha$ which is proportional to the BRDF.

Let us establish a Cartesian coordinate system $\mathbf{i}, \mathbf{j}, \mathbf{k}$ where $\mathbf{k} = \mathbf{V}$, and:

$$\mathbf{i} = \frac{\mathbf{V} \times \mathbf{N}}{|\mathbf{V} \times \mathbf{N}|}, \qquad \mathbf{j} = \mathbf{i} \times \mathbf{k}. \quad (21)$$

Using these unit vectors, the mirror direction $\mathbf{R}_m$ is:

$$\mathbf{R}_m = \sin\alpha_m \cdot \cos\phi_m \cdot \mathbf{i} + \sin\alpha_m \cdot \sin\phi_m \cdot \mathbf{j} + \cos\alpha_m \cdot \mathbf{k}. \quad (22)$$

From the mirror direction the light vector can be derived easily: $\mathbf{L}_m = ((\mathbf{N}\cdot\mathbf{R})_m\mathbf{N} - \mathbf{R}_m$. Note that sampling according to this probability density may generate directions that point into the object ($(\mathbf{N}\cdot\mathbf{L})_m < 0$). Thus we should check whether or not the light vector points out of the object ($(\mathbf{N}\cdot\mathbf{L})_m \geq 0$) and reject this sample if it does not. This rejection poses no problem since from these directions $L^{\mathrm{in}}(\mathbf{L}_m)$ is zero, thus these samples would get zero weight.

Summarizing, the Monte-Carlo estimate of the output radiance is

$$L^{\mathrm{out}}(\mathbf{V}) \approx \frac{1}{M}\cdot\frac{2\pi c_n}{n+1}\cdot\sum_{m=1}^{M} L^{\mathrm{in}}(\mathbf{L}_m)\cdot\cos\Theta_{\mathbf{L}_m}. \quad (23)$$

If c_n is the maximum allowed by inequality 6, then we obtain

$$L^{\mathrm{out}}(\mathbf{V}) \approx \frac{1}{M}\cdot\frac{n+2}{n+1}\cdot\sum_{m=1}^{M} L^{\mathrm{in}}(\mathbf{L}_m)\cdot\cos\Theta_{\mathbf{L}_m}. \quad (24)$$

The selected probability density is not optimally proportional to the integrand, only with $\cos^n\alpha$. It would be better to find a density that is proportional to $\cos^n\alpha\cdot\cos\Theta_{\mathbf{L}}$, but it would be quite complicated to implement practically. This simplification reduces the efficiency of the importance sampling, since the ignored $\cos\Theta_{\mathbf{L}}$ can be arbitrarily small at grazing angles, and its average is only $1/2$.

4.2. Importance sampling for the new model

The efficiency of the importance sampling gets higher for the new model, and it will be particularly good for large viewing angles. For the new model the integrand is

$$I(\mathbf{L},\mathbf{V}) = L^{\mathrm{in}}(\mathbf{L})\cdot c_n\cdot\frac{\cos^n\alpha}{\max(\cos\Theta_{\mathbf{L}},\cos\Theta_{\mathbf{V}})}\cdot\cos\Theta_{\mathbf{L}},$$

which can be simplified if the cases when the incident angle is smaller than the viewing angle ($\cos\Theta_{\mathbf{L}} \geq \cos\Theta_{\mathbf{V}}$) and when the incident angle is greater than the viewing angle ($\cos\Theta_{\mathbf{L}} < \cos\Theta_{\mathbf{V}}$) are considered separately:

$$I(\mathbf{L},\mathbf{V}) = L^{\mathrm{in}}(\mathbf{L})\cdot c_n\cdot\cos^n\alpha \quad \text{if } \Theta_{\mathbf{L}} \leq \Theta_{\mathbf{V}},$$
$$I(\mathbf{L},\mathbf{V}) = L^{\mathrm{in}}(\mathbf{L})\cdot c_n\cdot\cos^n\alpha\cdot\frac{\cos\Theta_{\mathbf{L}}}{\cos\Theta_{\mathbf{V}}} \quad \text{if } \Theta_{\mathbf{L}} > \Theta_{\mathbf{V}}.$$

As for the Phong model, the samples are generated according to $\frac{n+1}{2\pi}\cos^n\alpha$ probability density function. Using the $c_n = (n+2)/2\pi$ substitution, the Monte-Carlo approximation of the integral is:

$$L^{\mathrm{out}}(\mathbf{V}) \approx \frac{1}{M}\cdot\frac{n+2}{n+1}\cdot$$
$$\left(\sum_{\Theta_{\mathbf{L}_m}\leq\Theta_{\mathbf{V}}}^{M} L^{\mathrm{in}}(\mathbf{L}_m) + \sum_{\Theta_{\mathbf{L}_m}>\Theta_{\mathbf{V}}}^{M} L^{\mathrm{in}}(\mathbf{L}_m)\cdot\frac{\cos\Theta_{\mathbf{L}_m}}{\cos\Theta_{\mathbf{V}}}\right). \quad (25)$$

For large viewing angles the samples will be in the first sum of equation 25. Note that the probability density also compensates for the $\cos\Theta_{\mathbf{L}}$ factor here, thus this results in a more effective importance sampling. The larger the viewing angle, the greater the efficiency (even if the probability of the rejected samples approaches 0.5). The worst case of the importance sampling of the new model is at zero degree viewing angle, where the efficiency degrades to that of the sampling of the Phong model, which is fortunately the best here.

4.3. Albedo at grazing angles

Note that for $L^{\mathrm{in}} = 1$ equation 17 gives the albedo function at illumination direction $\mathbf{V}$, thus the importance sampling can also be used to effectively calculate and tabulate the values of the albedo function.

Equation 25, that calculates the albedo as an expected value, can also be given an intuitive explanation. At 90 degree viewing direction, the weight of sample rays is $(n+2)/(n+1)$. Since the BRDF is symmetric around $\mathbf{R}$, half of the samples point into the object, and are thus rejected. Consequently, the albedo at 90 degrees is:

$$\tilde{a}(90^\circ) = \frac{n+2}{2(n+1)}. \quad (26)$$

The albedos at grazing angles for $n = 1$, $n = 2$ and $n \to \infty$ are 3/4, 2/3 and 1/2, respectively. Note that for $n \to \infty$ which represents the ideal mirror case, for any $\epsilon > 0$, $\tilde{a}(90^\circ - \epsilon) = 1$, thus the new model can really converge to the ideal mirror.

5. Visualization of real materials

5.1. Metals

Metals have negligible diffuse reflectance and their BRDF is proportional to the Fresnel function which is based on a complex and wavelength dependent refraction index κ [5]. The Fresnel function also depends on the incident angle making the highlights colored. The reflected color can be computed as a product of the irradiance and the BRDF, which is usually done at a few discrete wavelengths.

For a single wavelength λ, the new BRDF for metals is:

$$f_r(\mathbf{L},\mathbf{V},\lambda) = \frac{n+2}{2\pi}\cdot\frac{\cos^n\alpha}{\cos\Theta_{\min}}\cdot F(\kappa(\lambda),\Theta(\mathbf{L},\mathbf{V})), \quad (27)$$

where $\Theta(\mathbf{L},\mathbf{V})$ is an appropriate incident angle, which should be a symmetric function of $\mathbf{L}$ and $\mathbf{V}$ to make the model reciprocal. A straightforward selection is the angle of the halfway vector $\mathbf{H}$. Another alternative is letting $\Theta = \Theta_{\min}$. This alternative gives back the angle of the halfway vector for the mirror direction but for other directions it generates a smaller angle. The largest difference between the angle of the halfway vector and $\Theta_{\min}$ occurs when the lighting is perpendicular to the surface and the viewing direction is parallel to it. Here $\Theta_{\min} = 0$ while the angle of the

halfway vector is 45°. Fortunately, the larger variation of Fresnel function is usually closer to 90° than to 0.

If we select $\Theta_{\min}$ to evaluate the Fresnel function, then the resulting BRDF is

$$f_{r,\mathrm{metal}}(\mathbf{L},\mathbf{V},\lambda) = \frac{n+2}{2\pi}\cdot\frac{\cos^n\alpha}{\cos\Theta_{\min}}\cdot F(\kappa(\lambda),\Theta_{\min}) = \frac{\cos^n\alpha}{g(\Theta_{\min})}, \quad (28)$$

where $g(\Theta_{\min})$ can be tabulated for the considered wavelengths. These tables allow for very fast BRDF evaluation. This computational cost is lower than that of any previously known metal models.

5.2. Plastics and ceramics

The new model is appropriate not only for metals but also for other highly specular materials, such as for certain plastics and ceramics. The main difference between these materials and metals is that their diffuse component is relevant and the specular part is responsible for the smaller part of the reflected power. For non metals the refraction index is a real number. The highlights can be assumed to be white everywhere not only for greater incident angles.

When rendering plastics, the classical Lambertian model can be applied for the diffuse component, while the specular part can be determined by the new model. Thus the BRDF has two components:

$$f_{r,\mathrm{plastics}}(\mathbf{L},\mathbf{V},\lambda) = \frac{a_d(\lambda)}{\pi} + a_s\cdot\frac{n+2}{2\pi}\cdot\frac{\cos^n\alpha}{\cos\Theta_{\min}}\cdot F(\kappa(\lambda),\Theta_{\min}), \quad (29)$$

where reflectivity a_d is the albedo of the diffuse component and a_s determines the size of the specular part. In order to make the model conserve energy, $a_s + a_d$ should not exceed 1. In many practical situations it is enough to compute the color on the three primary colors (r,g,b) and the Fresnel function can be assumed to be constant 1. For this simplified case the following plastic model is proposed:

$$f_{r,\mathrm{plastics}}(\mathbf{L},\mathbf{V}) = \frac{(r,g,b)}{\pi} + a_s\cdot\frac{n+2}{2\pi}\cdot\frac{\cos^n\alpha}{\cos\Theta_{\min}}\cdot(1,1,1), \quad (30)$$

where r,g,b are the albedos of the diffuse component at the wavelengths of the three primaries, and $a_s \le 1 - \max(r,g,b)$ should hold. It should be noted that not all non-metal materials can be visualized by this simple BRDF, and more sophisticated plastic models [16] might be required. However, this is a computationally effective model for many practical cases.

6. Material editor

Due to its simplicity, the proposed BRDF can be used in commercial rendering programs. Based on Paul Heckbert's BRDF editor [8], we have developed a material editor, where the optical parameters can be set interactively while the effect of the current settings is visualized by a simple scene. In the simplest case, the material editor displays a sphere that is illuminated by a few point lightsources and also by ambient light. The classical ambient term, however, is not good to render the objects outside the highlight spots since it would result in a constant color. Thus we propose the application of *homogeneous sky-light illumination* to replace classical ambient lighting model. The homogeneous sky-light illumination can be defined by the constant $L^{\mathrm{in}}(\mathbf{L}) = S_\lambda$ function at each representative wavelength. In this case the perceived radiance reflected to direction $\mathbf{V}$ is

$$L_\lambda^{\mathrm{out}}(\mathbf{V}) = \int_\Omega S_\lambda\cdot f_r(\mathbf{L},\mathbf{V},\lambda)\cdot\cos\Theta_{\mathbf{L}}\,d\omega_{\mathbf{L}} = S_\lambda\cdot a(\mathbf{V}), \quad (31)$$

which is the albedo of the material multiplied by the radiance of the sky. Note that even without point lightsources the resulting image is not homogeneous for a metal sphere due to the angle dependence of the Fresnel and the albedo functions (figure 7). Using precomputed albedo tables the evaluation of the sky-light illumination is fast.

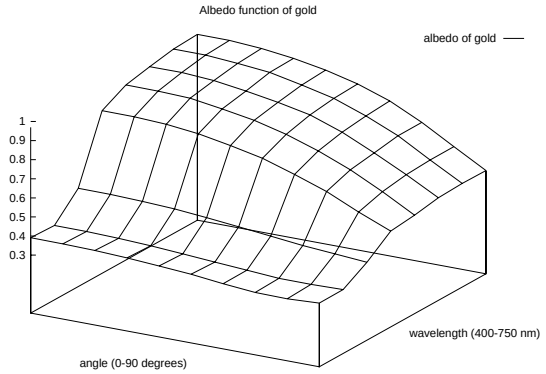

Figure 7: *The albedo of gold as a function of the incident angle and wavelength*

The sky-light as well as the point lightsources can be either white or colored, and can be set interactively by the user.

Since the material editor is expected to provide realistic appearance in all lighting conditions, the editor should incorporate automatic color mapping. This is done by calculating the illumination of a diffuse gray sphere, which is expected to have 0.5 median lightness on the display. This determines a scaling factor for the mapping of the images. Using the $\max(r,g,b)$ instead of the lightness, satisfactory results can be obtained for colored lightsources as well.

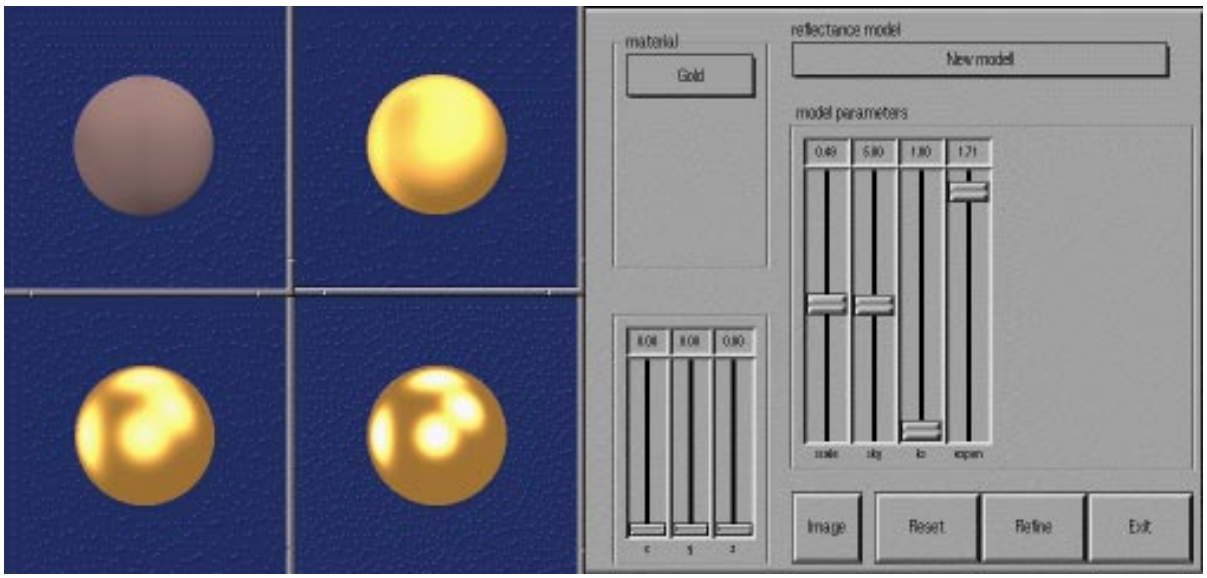

Figure 8: *A snapshot of the material editor displaying the diffuse gray reference object, and golden spheres having $n = 2, 8, 16$ exponents*

7. Reflectance models of $(\mathbf{N} \cdot \mathbf{H})$ type

7.1. Blinn model

The Blinn model can be modified similarly as the Phong model was corrected. Recall that the specular part the original Blinn model [3] is

$$f_{r,\mathrm{Blinn}}(\mathbf{L}, \mathbf{V}) = C_n \cdot (\mathbf{N} \cdot \mathbf{H})^n. \qquad (32)$$

The analytical calculation of the C_n constant for integer n values can be found in [1]. The complexity of this calculation is $O(n)$. The problems of this model are similar to that of the Phong model. The reflected radiance and the albedo converges to zero at grazing angles if n goes to infinity.

Similarly to the procedures applied for the Phong model, this model can also be corrected:

$$f_r(\mathbf{L}, \mathbf{V}) = C_n \cdot \frac{(\mathbf{N} \cdot \mathbf{H})^n}{\max((\mathbf{N} \cdot \mathbf{L}), (\mathbf{N} \cdot \mathbf{V}))}. \qquad (33)$$

The C_n constants that can be allowed not to violate energy balance are summarized by table 1.

n	Blinn	Blinn/ $\cos\Theta_{\min}$
1	0.350	0.293
2	0.382	0.368
4	0.449	0.449
8	0.592	0.592
16	0.895	0.895
32	1.52	1.52
64	2.79	2.79
128	5.34	5.34
256	10.4	10.4
512	20.6	20.6

Table 1: *The maximum C_n constants for the original and the corrected Blinn models*

7.2. Ward model

Ward [21] introduced a simple BRDF of type $(\mathbf{N} \cdot \mathbf{H})$. This model is simpler than other known metal models and its anisotropic form could provide particularly good metallic impression. For the isotropic case, the specular component has the following form:

$$f_r(\mathbf{L}, \mathbf{V}) = \frac{C_{\max}}{4\pi m^2} \cdot \frac{\exp\left(-\tan^2 \delta / m^2\right)}{\sqrt{((\mathbf{N} \cdot \mathbf{L})(\mathbf{N} \cdot \mathbf{V}))}}, \qquad (34)$$

where $\delta = \arccos(\mathbf{N} \cdot \mathbf{H})$ and m is the standard deviation (RMS) of the surface slope.

The main problem of this model is its behavior at grazing angles and at viewing directions below the mirror direction. Not only the BRDF but also the reflected radiance are unbounded for the Ward model, which is against practical considerations. Ward stated that selecting $C_{\max} = 1$ the model meets energy balance if $m < 0.2$. Examining the albedo

function in the range of $0...89^\circ$, this is true quite accurately. Here the maximum of the albedo is greater than 0.85, and it converges to 1 if m is decreased.

However at grazing angles the albedo significantly violates energy balance (figure 4). In the next section, it will be be shown analytically that the BRDF diverges to infinity at grazing angles, thus this model is not physically plausible. For example, if $m = 0.1$, then $a(89.995^\circ) = 1.2$, $a(89.999^\circ) = 2.6$ and $a(89.9995^\circ) = 3.8$.

One way of correcting this error is the limitation of the $1/\sqrt{(\mathbf{N}\cdot\mathbf{L})\cdot(\mathbf{N}\cdot\mathbf{V})}$ function.

On the other hand, the previously applied normalization can also be used here, which leads to a new BRDF model:

$$f_r(\mathbf{L},\mathbf{V}) = \frac{C_{\max}}{4\pi m^2}\cdot\frac{\exp\left(-\tan^2\delta/m^2\right)}{\max((\mathbf{N}\cdot\mathbf{L}),(\mathbf{N}\cdot\mathbf{V}))}, \qquad (35)$$

A similar method can be applied to the anisotropic Ward model as well.

The $C_{\max}$ constants are summarized by table 2.

m	$C_{\max}$
0.4	1.63
0.2	1.16
0.1	1.04
0.05	1.011
0.02	1.005
0.01	1.002
0.005	1.002

Table 2: *The maximum $C_{\max}$ constants for the corrected Ward models*

7.3. Cook-Torrance model

Assuming that the Fresnel factor is 1, the BRDF of the Cook-Torrance model [4] is

$$f_r(\mathbf{L},\mathbf{V}) = \frac{\exp\left(-\tan^2\delta/m^2\right)}{4\pi m^2\cos^4\delta}\cdot\frac{G(\mathbf{N},\mathbf{L},\mathbf{V})}{(\mathbf{N}\cdot\mathbf{L})(\mathbf{N}\cdot\mathbf{V})}, \quad (36)$$

where the *geometry factor* $G(\mathbf{N},\mathbf{L},\mathbf{V})$ [19] is

$$G = \min\{2\cdot\frac{(\mathbf{N}\cdot\mathbf{H})(\mathbf{N}\cdot\mathbf{V})}{(\mathbf{V}\cdot\mathbf{H})}, 2\cdot\frac{(\mathbf{N}\cdot\mathbf{H})(\mathbf{N}\cdot\mathbf{L})}{(\mathbf{L}\cdot\mathbf{H})}, 1\}. \qquad (37)$$

As the Ward model, the Cook-Torrance model is not physically plausible either since it violates the energy balance at grazing angles (figure 4) as it is shown analytically that the albedo goes to infinity at grazing angles. Illustrating the divergence numerically for $m = 0.1$, the albedo values at $\Theta_{\mathbf{L}} = 89.9^\circ$, $\Theta_{\mathbf{L}} = 89.99^\circ$ and $\Theta_{\mathbf{L}} = 89.999^\circ$ are 2.1, 9.3 and 91 respectively. On the other hand, both the BRDF and the reflected radiance diverge. A possible correction is the limitation of the BRDF or more precisely the $G/((\mathbf{N}\cdot\mathbf{L})\cdot(\mathbf{N}\cdot\mathbf{V}))$ term.

7.4. Proof of the divergence of the Cook-Torrance and Ward models

Let us consider the situation around the highlight close to the grazing angles, that is where $\mathbf{V}\approx\mathbf{R}$, $\mathbf{H} = (\mathbf{L}+\mathbf{V})/|\mathbf{L}+\mathbf{V}|\approx\mathbf{N}$, $\mathbf{NL}\approx 0$ and $\mathbf{NV}\approx 0$. We have to show that it is possible to move $\mathbf{L}$ towards grazing angles in a way that the albedo will diverge along this path. An appropriate path is a sufficiently small arc of the main circle of the directional hemisphere. For a given vector $\mathbf{L}$, the albedo integral requires the consideration of all vectors $\mathbf{V}$. However, establishing a lower bound, only those viewing vectors are considered which, together with $\mathbf{L}$ result in those $\mathbf{H}$ halfway vectors that are inside a *cap* (spherical circle around $\mathbf{N}$) (figure 9). Since $\mathbf{H} = (\mathbf{L}+\mathbf{V})/|\mathbf{L}+\mathbf{V}|$ should hold, the allowable domain of viewing vectors $\mathbf{V}$ can be determined from these two regions by "spherical mirroring" of each point in the domain of $\mathbf{L}$ onto each point in the domain of $\mathbf{H}$. The left figure demonstrates that if the domain of $\mathbf{L}$ is too big compared to that of $\mathbf{H}$, then those $\mathbf{V}$ vector sets which correspond to different $\mathbf{L}$ vectors will not have a common intersection. However, if the domain of $\mathbf{L}$ is small compared to that of $\mathbf{H}$, then the $\mathbf{V}$ vector sets corresponding to different $\mathbf{L}$ vectors will have a common intersection (right figure 9). This region of intersection constrained to the the upper hemisphere is called the *critical region.*

In the Ward model, factor $(1/4\pi m^2)\cdot\exp\left(-\tan^2\delta/m^2\right)$ can be lowerbounded inside the *cap*, so can the $(1/4\pi m^2\cos^4\delta)\cdot\exp\left(-\tan^2\delta/m^2\right)$ factor of the Cook-Torrance model. Thus we can find appropriate positive constants μ_{Ward}, and μ_{Cook} so that

$$\frac{1}{4\pi m^2}\cdot\exp\left(-\tan^2\delta/m^2\right)\geq\mu_{\mathrm{Ward}},$$

$$\frac{1}{4\pi m^2\cos^4\delta}\cdot\exp\left(-\tan^2\delta/m^2\right)\geq\mu_{\mathrm{Cook}}. \qquad (38)$$

Considering the geometry term and the denumerator of the Cook-Torrance model, we can further restrict the domain of $\mathbf{L}$ and the *cap* for $\mathbf{H}$ to guarantee that the constant 1 is the real minimum in the geometry term, thus here we can apply the following substitution

$$\frac{G(\mathbf{N},\mathbf{L},\mathbf{V})}{(\mathbf{N}\cdot\mathbf{L})(\mathbf{N}\cdot\mathbf{V})} = \frac{1}{(\mathbf{N}\cdot\mathbf{L})(\mathbf{N}\cdot\mathbf{V})}. \qquad (39)$$

Using the constant lower bounds valid inside the *cap*, we can obtain:

$$\frac{\mu_{\mathrm{Ward}}}{\sqrt{(\mathbf{N}\cdot\mathbf{L})(\mathbf{N}\cdot\mathbf{V})}}\leq f_{r,\mathrm{Ward}}(\mathbf{L},\mathbf{V}),$$

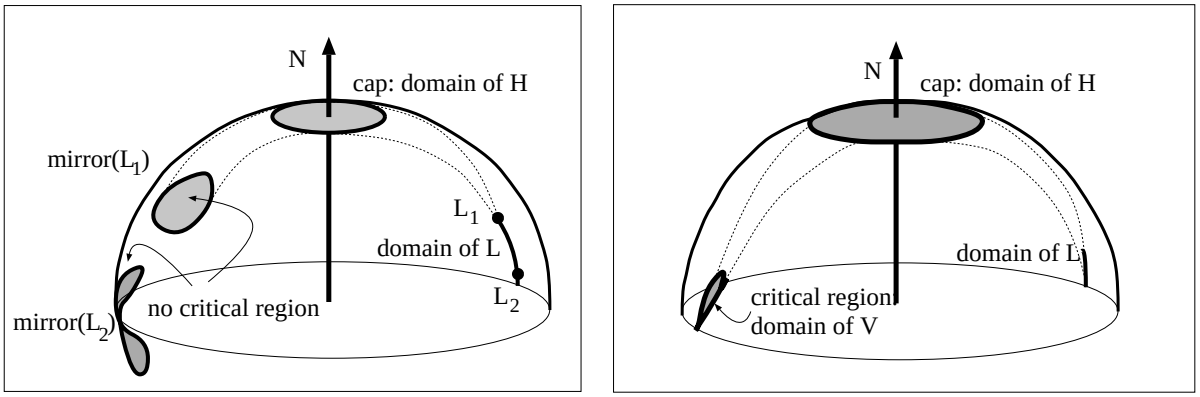

Figure 9: *The relations between the domains of* $\mathbf{L}$, $\mathbf{H}$ *and* $\mathbf{V}$ *vectors (left figure: domain of* $\mathbf{L}$ *is too big compared to the domain of* $\mathbf{H}$*; right figure: domain of* $\mathbf{L}$ *is small compared to the domain of* $\mathbf{H}$*)*

$$\frac{\mu_{\mathrm{Cook}}}{(\mathbf{N}\cdot\mathbf{L})(\mathbf{N}\cdot\mathbf{V})} \leq f_{r,\mathrm{Cook}}(\vec{L},\vec{V}). \tag{40}$$

For the albedo, a lowerbound can be established by bounding the hemispherical domain Ω to the *critical region* $\Omega_{\mathrm{critical}}$ and using inequality (40). Let us consider the Ward model:

$$a_{\mathrm{Ward}}(\mathbf{L}) \geq \int\limits_{\Omega_{\mathrm{critical}}} \frac{\mu_{\mathrm{Ward}}}{\sqrt{(\mathbf{N}\cdot\mathbf{L})(\mathbf{N}\cdot\mathbf{V})}}\cdot(\mathbf{NV})\; d\omega_{\mathbf{V}} =$$

$$\frac{\mu_{\mathrm{Ward}}}{\sqrt{(\mathbf{N}\cdot\mathbf{L})}} \int\limits_{\Omega_{\mathrm{critical}}} \sqrt{(\mathbf{N}\cdot\mathbf{V})}\; d\omega_{\mathbf{V}}. \tag{41}$$

For the albedo of the Cook-Torrance model, we can obtain:

$$a_{\mathrm{Cook}}(\mathbf{L}) \geq \int\limits_{\Omega_{\mathrm{critical}}} \frac{\mu_{\mathrm{Cook}}}{(\mathbf{N}\cdot\mathbf{L})(\mathbf{N}\cdot\mathbf{V})}(\mathbf{N}\cdot\mathbf{V})\; d\omega_{\mathbf{V}} =$$

$$\frac{\mu_{\mathrm{Cook}}}{(\mathbf{N}\cdot\mathbf{L})}\cdot|\Omega_{\mathrm{critical}}|. \tag{42}$$

Since at grazing angles $(\mathbf{NL})$ converges to zero, the lowerbounds in equations (41) and (42) diverge, which forces the albedo of the Ward and Cook-Torrance models to diverge as well.

7.5. Mean albedo

If the irradiance L^{in} is constant in the whole hemisphere, then the ratio of the total reflected power is called the *mean albedo*, which can be obtained as:

$$a_{\mathrm{mean}} = \frac{1}{\pi}\cdot\int\limits_{\Omega} a(\mathbf{L})\cdot\cos\Theta_{\mathbf{L}}\; d\omega_{\mathbf{L}}. \tag{43}$$

For diffuse white materials and for the ideal mirror the mean albedo is 1. Table 3 shows the mean albedo for different models.

n	Phong	$\frac{\text{Phong}}{\cos\Theta_{\min}}$	Blinn	$\frac{\text{Blinn}}{\cos\Theta_{\min}}$
1	0.737	0.934	0.879	0.941
2	0.708	0.902	0.800	0.952
4	0.688	0.887	0.706	0.863
8	0.676	0.888	0.620	0.748
16	0.670	0.901	0.562	0.679
32	0.668	0.919	0.531	0.648
64	0.667	0.937	0.516	0.639
128	0.667	0.953	0.508	0.640
256	0.667	0.966	0.504	0.644
512	0.667	0.975	0.502	0.649
∞	0.5	1	0.5	1

Table 3: *Mean albedo values of different models*

The proposed correction by $1/\cos\Theta_{\min}$ has "pumped-up" the mean albedo, especially for the Phong-type model. The models of $(\mathbf{N}\cdot\mathbf{H})$ type including the Blinn and the Ward models are significantly "darker" even after the pumping-up than the Phong-type models that converge to the ideal mirror faster by increasing n. For example, if $n = 128$, then the mean albedo of the Blinn model has been increased from 0.508 to 0.640 due to the correction. At 90 degree incident angle, on the other hand, the albedo has changed from $7.8\cdot10^{-3}$ just to $3.7\cdot10^{-2}$.

8. Simulation results

The following images have been rendered by a Monte-Carlo ray-tracing algorithm that incorporates the discussed importance sampling.

The first three images display metal objects and were rendered by the metal model of equation 28. Color computation was carried out at 8 discrete wavelengths, then using the color matching functions the XYZ primaries were generated, which were finally converted to RGB. The material properties of the metals (complex index of refraction), color matching functions and the XYZ to RGB conversion matrix were taken from [5].

Figure 10 shows different metal objects on a diffuse plate. There are three point lightsources and sky-light illumination is also present.

Figure 11 displays three metal teapots on a diffuse plane. Note that the teapot in the middle has quite high n value, creating mirror images of the other two teapots.

Figure 12 displays a golden Beethoven head of relatively low n value (4). On the other hand, the base silver plate acts as an non-perfect mirror since it has very high n value (5000) and the Fresnel function of the silver is close to 1, thus the mirror images of the other objects are just slightly blurred.

The last two images were rendered by the plastic model of equation 30. Figure 13 shows plastic spheres on a plastic plate. All spheres have a large diffuse component defining colors of the same hue but different lightness and saturation, and the (a_s, n) specular parameters are selected according to the following sequence: $(0.04, 169)$, $(0.065, 64)$, $(0.09, 9)$, $(0.13, 3)$.

Figure 14 shows two ceramic teapots. Again, the diffuse component is dominant, the n exponents are 100 and 20, respectively.

9. Conclusions

The paper derived a very simple BRDF model from the reciprocal Phong model, that can render metals and other specular objects. The new model is particularly suitable for importance sampling in Monte-Carlo ray-tracing algorithms. Importance sampling of the new model is simpler than that of the Blinn and Ward models and more efficient than that of the reciprocal and non-metallic Phong model. The new model can arbitrarily well approximate the ideal mirror, thus mirrors and polishing do not require a special case.

Using numerical (Monte-Carlo) integration and also analytical considerations that are not detailed in the paper, we have shown that the Ward and the Cook-Torrance models are not physically plausible since they cannot conserve energy at grazing angles. The albedo, BRDF and the reflected radiance are unbounded. The problems of the behavior at grazing angles and energy conservation of physically based and physically plausible models require further research. No physically based model exists that can solve all problems at grazing angles. The proposed limitation of the BRDF of these models can guarantee physical plausibility, but is not appropriate for the representation of very smooth metals.

We have shown that multiplying different known BRDFs by $1/\cos\Theta_{\min}$ the new model preserves energy balance and can provide metallic impression. These models can easily be incorporated in rendering software.

We have proposed sky-light illumination to replace the ambient term when rendering a convex object and discussed how this can be computed efficiently using tabulated albedo values.

An important subject of the future research is the fitting to measured BRDF data. The models proposed in this paper have the general form $f(\alpha)/g(\Theta_{\min})$ where f is some BRDF and g is a scalar function. If measurement data are available, function g can also be determined to fit the resulting BRDF to the measurement results. On the other hand, if there is no such measurement data, the new model can be fitted to some physically accurate BRDF, as for example, to the He-Torrance or the Cook-Torrance models. The benefit of such an approach is that function g can be tabulated as a result of the fitting and the new model can be evaluated much more efficiently than the reference models.

The paper discussed the anisotropic p-models that include the Lafortune's model as a special case. Thus the new model is expected to provide more accurate fitting with less number of terms. In such fitting the resulting albedo should also be used as a control parameter in addition to the BRDF values.

10. Acknowledgments

The authors thank Paul Heckbert (Carnegie-Mellon) for providing his BRDF editor [8] and Eric Lafortune (Cornell) for his helpful comments.

References

1. J. Arvo. Application of irradiance tensors to the simulation of non-lambertian phemomena. In *Computer Graphics (SIGGRAPH '95 Proceedings)*, pages 335–342, 1995.

2. Petr Beckmann and Andre Spizzichino. *The Scattering of Electromagnetic Waves from Rough Surfaces.* MacMillan, 1963.

3. James F. Blinn. Models of light reflection for computer synthesized pictures. In *Computer Graphics (SIGGRAPH '77 Proceedings)*, pages 192–198, 1977.

4. R. Cook and K. Torrance. A reflectance model for computer graphics. *Computer Graphics*, 15(3), 1981.

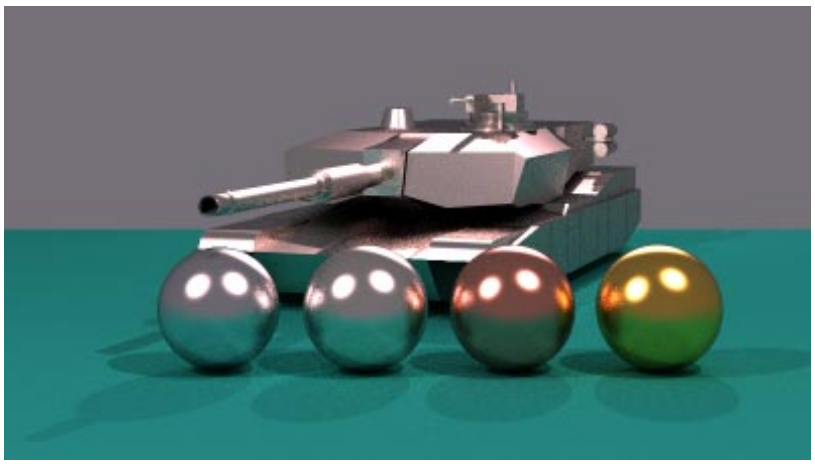

Figure 10: *A silver tank ($n = 20$) with aluminum ($n = 40$), silver ($n = 50$), copper ($n = 50$) and golden ($n = 40$) spheres*

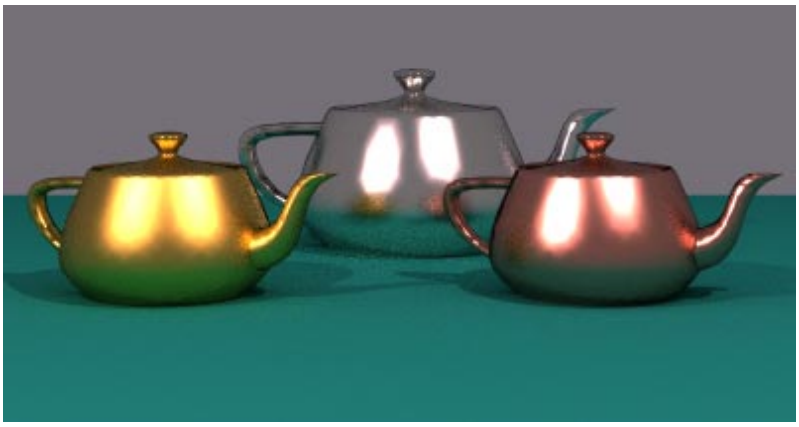

Figure 11: *A golden ($n = 10$), silver ($n = 190$) and copper ($n = 100$) teapots*

5. A. Glassner. *Principles of Digital Image Synthesis*. Morgan Kaufmann Publishers, Inc., San Francisco, 1995.
6. B. Hapke. A theoretical photometric function for the lunar surface. *Journal of Geophysical Research*, 68(15), 1963.
7. X. He, K. Torrance, F. Sillion, and D. Greenberg. A comprehensive physical model for light reflection. *Computer Graphics*, 25(4):175–186, 1991.
8. P. Heckbert. Brdf viewer, http: //www.cs.cmu.edu/ afs/ cs.cmu.edu/ user/ph/ www/src/illum. 1997.
9. D. S. Immel, M. F. Cohen, and D. P. Greenberg. A radiosity method for non-diffuse environments. In *Computer Graphics (SIGGRAPH '86 Proceedings)*, pages 133–142, 1986.
10. E. Ken. Reflectance phenomenology and modeling tutorial. 1994. http://www.erim.org.
11. E. Lafortune. Verbal communication. 1997.
12. E. Lafortune, S. Foo, K. Torrance, and D. Greenberg. Non-linear approximation of reflectance functions. *Computer Graphics (SIGGRAPH '97 Proceedings)*, pages 117–126, 1997.
13. E. Lafortune and Y. D. Willems. Using the modified phong reflectance model for physically based rendering. Technical Report RP-CW-197, Department of Computing Science, K.U. Leuven, 1994.
14. R. Lewis. Making shaders more physically plausible. In *Rendering Techniques '93*, pages 47–62, 1993.
15. M. Minnaert. The reciprocity principle in lunar photometry. *Astrophysical Journal*, 93:403–410, 1941.
16. M. Oren and S. Nayar. Generalization of lambert's re-

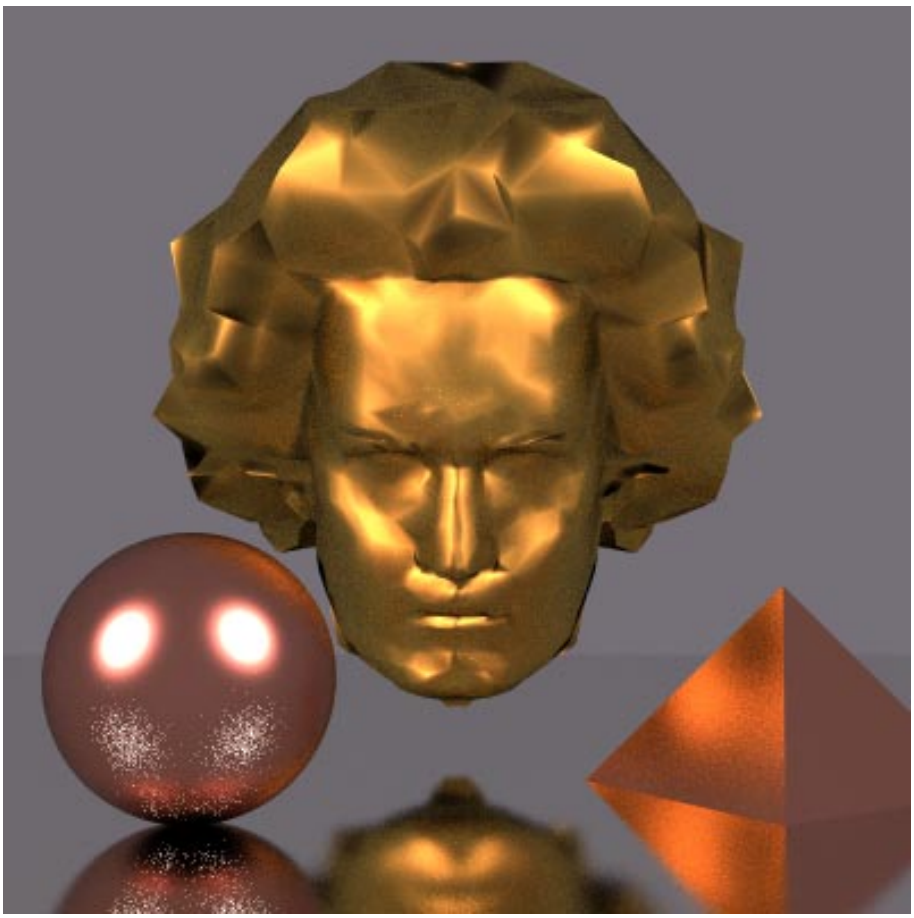

Figure 12: *A golden Beethoven ($n = 4$) with a copper sphere ($n = 40$) and a copper pyramid ($n = 150$) on a silver mirror ($n = 5000$)*

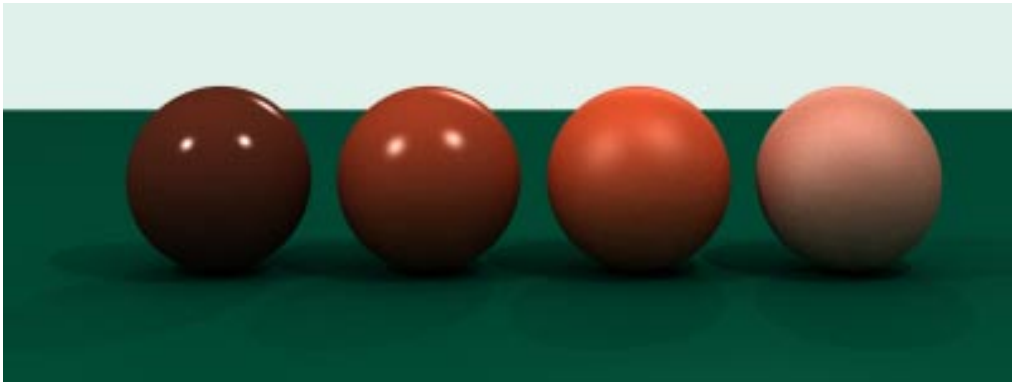

Figure 13: *Plastic objects*

Figure 14: *Ceramic teapots*

flectance model. *Computer Graphics (SIGGRAPH '94 Proceedings)*, pages 239–246, 1994.

17. Bui Thong Phong. Illumination for computer generated images. *Communications of the ACM*, 18:311–317, 1975.
18. P. Poulin and A. Fournier. A model for anisotropic reflection. *Computer Graphics*, 24(4):273–281, 1990.
19. L. Szirmay-Kalos (editor). *Theory of Three Dimensional Computer Graphics.* Akadémia Kiadó, Budapest, 1995.
20. K. Torrance and M. Sparrow. Off-specular peaks in the directional distribution of reflected thermal distribution. *Journal of Heat Transfer — Transactions of the ASME*, pages 223–230, May 1966.
21. G. Ward. Measuring and modeling anisotropic reflection. *Computer Graphics*, 26(2):265–272, 1992.